Quantum Wave Packet Study of the $H^+ + D_2$ Reaction on Diabatic Potential Energy Surfaces

Rui-Feng Lu, Tian-Shu Chu, and Ke-Li Han*

State Key Laboratory of Molecular Reaction Dynamics, Dalian Institute of Chemical Physics, Chinese Academy of Sciences, Dalian 116023, China

Received: April 20, 2005; In Final Form: June 2, 2005

The exact three-dimensional nonadiabatic quantum dynamics calculations were carried out for the title reaction by a time-dependent wave packet approach based on a newly constructed diabatic potential energy surface (Kamisaka et al. *J. Chem. Phys.* **2002**, *116*, 654). Three processes including those of reactive charge transfer, nonreactive charge transfer, and reactive noncharge transfer were investigated to determine the initial state-resolved probabilities and reactive cross sections. The results show that a large number of resonances can be observed in the calculated probabilities due to the deep well on adiabatic ground surface and the dominant process is the reactive noncharge-transfer process. Some interesting dynamical features such as v-dependent and j-dependent behaviors of the probabilities are also revealed. In addition, a good agreement has been achieved in the comparison between the calculated quantum cross sections from the ground rovibrational initial state and the experimental measurement data.

I. Introduction

Electronically nonadiabatic transitions and their dynamical effects on chemical reactions have recently become very hot issues,[1−7] and considerable efforts have been made in the development of experimental techniques and theoretical schemes to deal with the problems involving two or more potential energy surfaces. In the nonadiabatic quantum dynamics field, the H_3^+ system, and its isotopic variants can serve as a paradigm for its simplicity (only three protons and two electrons) and its yet rich dynamics information. This ion−molecular system has three reaction channels, the reactive charge transfer (RCT), the nonreactive charge transfer (NRCT), and the reactive noncharge transfer (RNCT) with the first two channels induced by the nonadiabatic transitions of the system. The underlying reaction mechanisms for this reaction and its isotopic variants have been extensively investigated in a large variety of experimental works and theoretical calculations.[8−21] In early experimental works, Teloy et al. reported their measured integral reaction cross sections for the $H^+ + D_2$ [9] and $D^+ + H_2$ [10] systems, while on the theoretical side both quantum mechanical (QM) methods and quasiclassical trajectory (QCT) methods have been developed and used in the nonadiabatic calculations for these reaction systems. Last et al.[11] calculated the cross sections and the opacity functions for the charge-transfer process in the $H + H_2^+$ reaction system, employing a time-independent method with coupled states approximation. Ushakov et al.[12] investigated the collinear $H^+ + H_2$ system within a time-independent framework, and revealed a strong dependence of the nonadiabatic transition probability on the initial vibrational state of reactant H_2. By using Johnson's hyperspherical coordinates and the iterative Lanczos reduction propagation technique in a time-dependent wave packet study, Markovic et al.[13−15] presented their results on the $D^+ + H_2$ system for the total angular momentum $J = 0$, but they met with the problem of slow convergence due to the deep well on the ground surface. Takayanagi and his co-works[16] used the hyperspherical coordinate approach in their QM calculations and the Tully's fewest switches (TFS) method in their QCT calculations, and presented the cumulative reaction probability for $J = 0$. Further, the cross sections for the $D^+ + H_2$, $D^+ + D_2$ and $H^+ + D_2$ collisions have been calculated by Ichihara et al.[17] using the TSH method on their ab initio 3×3 diatomics-in-molecule (DIM) PES[18] and the comparison between the calculated results and the experimental data revealed the necessity of performing more accurate quantum calculations for these reaction systems. A substantially extended work of the previous studies for the $D^+ + H_2$ reaction was made by Kamisaka et al.,[19] and they calculated the cumulative transition probabilities for $J = 0$ for six adiabatic and nonadiabtic processes of the $(DH_2)^+$ system by time-independent quantum approach based on their newly construct potential energy surfaces. Very recently, we have carried out an exact three-dimensional wave packet studies for the $D^+ + H_2$ reaction utilizing an extended split operator scheme (XSOS).[20] Our results demonstrated that the centrifugal sudden (CS) approximation is actually inadequate for this reaction system and the close-coupled (CC) cross sections agree reasonably well with the experimental values.

Extending on the recent work mentioned above, in this paper, we performed the study for the ion−molecule collisions of H^+ with D_2, since the $H^+ + D_2$ reaction has not been extensively subjected to thorough theoretical studies and no exact quantum results comparable to experimental observables have been achieved thus far. The quantum wave packet was propagated over a collision energy range of 1.7−2.5 eV with the same diabatic KBNN potential energy surface as that in ref 19, which was a newly constructed surface consisting of 3×3 DIM potential matrix and three-body correction terms. By diagonalizing the KBNN potential matrix, we obtained the three adiabatic potential energy surfaces, the ground $1^1A'$ surface with a deep well of about 4.0 eV, and two repulsive first and second excited surfaces $2^1A'$ and $3^1A'$. The crossing seams between $1A'$ and $2A'$ surfaces lies in the region far away from the geometry of

* Corresponding author. E-mail: klhan@dicp.ac.cn.

10.1021/jp0520401 CCC: $30.25 © 2005 American Chemical Society
Published on Web 07/13/2005

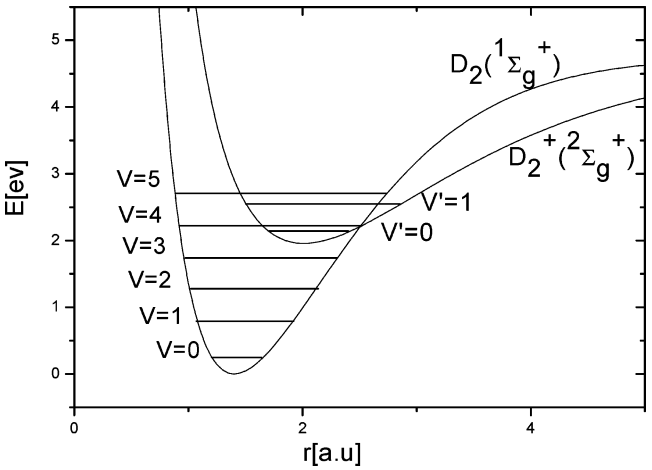

Figure 1. Potential energy curves of the isolated D_2 and D_2^+ with the vibrational energy levels (rotational quantum number of a diatomic molecule is zero).

the $(HD_2)^+$ complex. Clearly, the presence of the singlet deep well, which is quite different from the abstraction reactions of F/Cl + H_2,[23−28] will definitely challenge the present accurate quantum calculations as being proved by the previous cases of the O + H_2,[29−32] H + O_2,[33,34] and C + H_2 [35,36] reactions. To better understand the role of the initial vibational excitation in the reaction dynamics, we show, in Figure 1, the potential curves of the diatomic molecules D_2 and D_2^+ with the depicted crossing point and vibrational energy levels. It can be seen clearly that $v = 4$ of D_2 and $v' = 0$ of D_2^+ are the closest vibrational levels to the crossing. In addition, the present investigated channels are the following three channels,

$$H^+ + D_2 \rightarrow D + HD^+ \text{ RCT} \tag{1.1}$$

$$H^+ + D_2 \rightarrow H + D_2^+ \text{ NRCT} \tag{1.2}$$

$$H^+ + D_2 \rightarrow D^+ + HD \text{ RNCT} \tag{1.3}$$

The organization of the paper is as follows. Section II briefly outlines the theory of the nonadiabatic time-dependent wave packet (TDWP) treatment for the multisurface problem. The calculated results and discussion are given in section III, and we present the concluding remarks in section IV.

II. Theory

Since the TDWP method has been well documented in numerous literature dealing with quantum scattering problems[37−41] and the present theoretical treatment for nonadiabatic couplings essentially follows our previous works,[42−45] here we only give a brief outline of this method with the extended split operator scheme.

The Hamiltonian of the triatomic system in terms of the reactant Jacobi coordinates can be written as (in atomic units)

$$H = -\frac{1}{2\mu_R}\frac{\partial^2}{\partial R^2} + \frac{(J-j)^2}{2\mu_R R^2} + \frac{j^2}{2\mu_r r^2} + V(R,r,\theta) + h(r) \tag{2.1}$$

where μ_R is the reduced mass between the atom and the diatom, μ_r is the reduced mass of D_2, J is the total angular momentum operator, and j is the rotational angular momentum operator of D_2. The interaction potential $V(R, r, \theta)$ is defined as $V_{KBNN} - V_r$, here V_r is the diatomic reference potential, part of the diatomic reference Hamiltonian $h(r)$

$$h(r) = -\frac{1}{2\mu_r}\frac{\partial^2}{\partial r^2} + V_r(r) \tag{2.2}$$

The time-dependent Schrödinger equation of the triatomic reaction system can be written as

$$i\frac{\partial}{\partial t}\Psi_i = H\Psi_i \tag{2.3}$$

where Ψ_i ($i = 1$, 2 or 3) is the component of the total unitary wave function relating to each of the three potential energy surfaces, each is expanded in terms of translational basis $U_n^v(R)$, vibrational basis $\phi_v(r)$, and the body-fixed (BF) total angular momentum eigenfunction $Y_{jK}^{JM\epsilon}(R,r)$.[38] Since the CS approximation has been found insufficient for an accurate quantum calculation on the $(DH_2)^+$ system,[20] it is also necessary to carry out the exact close-coupled (CC) calculation for the present system. In the CC calculation, the operation of the orbital angular momentum (or centrifugal potential) operator on the BF total angular momentum eigenfunction can be expressed as[46,47]

$$\frac{1}{2\mu_R R^2}\langle Y_{jK}^{JM\epsilon}|(J-j)^2|Y_{j'K'}^{JM\epsilon}\rangle = \frac{1}{2\mu_R R^2}\delta_{jj'}\{[J(J+1) + j(j+1) - 2K^2]\delta_{KK'} - \lambda_{JK}^+\lambda_{jK}^+(1+\delta_{K0})^{1/2}\delta_{K+1,K'} - \lambda_{JK}^-\lambda_{jK}^-(1+\delta_{K1})^{1/2}\delta_{K-1,K'}\} \tag{2.4}$$

and λ is defined as

$$\lambda_{AB}^{\pm} = [A(A+1) - B(B\pm 1)]^{1/2} \tag{2.5}$$

Thus, through the centrifugal potential, different K channels can be coupled for the total angular momentum $J > 0$.

The initial Gaussian wave packet is propagated by an extended split operator scheme (XSOS)

$$\begin{bmatrix}\psi_1(t+\Delta)\\ \psi_2(t+\Delta)\\ \psi_3(t+\Delta)\end{bmatrix} = e^{-iH_0\Delta/2}e^{-iV_{rot}\Delta/2}e^{-i\begin{bmatrix}V_{11} & V_{12} & V_{13}\\ V_{21} & V_{22} & V_{23}\\ V_{31} & V_{32} & V_{33}\end{bmatrix}\Delta}e^{-iV_{rot}\Delta/2}e^{-iH_0\Delta/2}\begin{bmatrix}\psi_1(t)\\ \psi_2(t)\\ \psi_3(t)\end{bmatrix}$$

$$= e^{-iH_0\Delta/2}e^{-iV_{rot}\Delta/2}Te^{-i\begin{bmatrix}V_1 & 0 & 0\\ 0 & V_2 & 0\\ 0 & 0 & V_3\end{bmatrix}\Delta}T^+e^{-iV_{rot}\Delta/2}e^{-iH_0\Delta/2}\begin{bmatrix}\psi_1(t)\\ \psi_2(t)\\ \psi 3(t)\end{bmatrix}$$

$$= e^{-iH_0\Delta/2}e^{-iV_{rot}\Delta/2}T\begin{bmatrix}e^{-iV_1\Delta} & 0 & 0\\ 0 & e^{-iV_2\Delta} & 0\\ 0 & 0 & e^{-iV_3\Delta}\end{bmatrix}T^+e^{-iV_{rot}\Delta/2}e^{-iH_0\Delta/2}\begin{bmatrix}\psi_1(t)\\ \psi_2(t)\\ \psi_3(t)\end{bmatrix} \tag{2.6}$$

where T is the orthogonal transform matrix, T^+ is the transposed and conjugated matrix of T, and Δ is the time step, and H_0 and V_{rot} are defined as follows:

$$H_0 = -\frac{1}{2\mu_R}\frac{\partial^2}{\partial R^2} + h(r) \tag{2.7}$$

$$V_{rot} = \frac{(J-j)^2}{2\mu_R R^2} + \frac{j^2}{2\mu_r r^2} \tag{2.8}$$

The initial-state specified total reaction probabilities are finally obtained on the surfaces of relevance by calculating the reaction flux at a fixed surface $s = s_0$,

$$P^J(E) = \sum_i \frac{1}{\mu} \mathrm{Im}\left[\left\langle \psi_i(E) \middle| \delta(s - s_0) \frac{\partial}{\partial s} \middle| \psi_i(E) \right\rangle\right] \quad (2.9)$$

for reactive process, $s = r$ and $\mu = \mu_r$; for nonreactive process, $s = R$ and $\mu = \mu_R$. The total reaction cross sections are calculated by

$$\sigma(E) = \frac{\pi}{k_0^2} \sum_J (2J + 1) P^J(E) \quad (2.10)$$

with $k_0 = \sqrt{2\mu_R E}$ and E is the collision energy.

III. Results and Discussion

The numerical parameters of the converged calculation are as follows: 300 translational basis functions for the R coordinate in the range of 0.2−20.0 a_0 (among them 140 for the interaction region). The center of the initial wave packet with the width of 0.35 a_0 is located at $R = 12.0$ a_0, and the initial wave packet has an average translational energy of 2.16 eV. 150 vibrational basis functions for the r coordinate from 0.5 to 17.0 a_0, $j_{max} = 100$ for rotational basis, in the asymptotic region, 10 D_2 vibrational basis functions and 130 pseudo-D_2 are used, the total propagation time is 35000 au, and the number of K used in the CC calculation is up to 5. A value of $J_{max} = 59$ was used in the summation which is sufficient to converge the cross sections in the investigated energy range. Besides, the much heavier $(HD_2)^+$ reaction system also made the present calculation a more tedious one as compared with the $(DH_2)^+$ system.

The calculated reaction probabilities for the ground rovibrational initial state of D_2 are shown in Figure 2. Because of the deep well on the ground surface, there many sharp, overlapping resonance peaks appeared in the reaction probabilities. As can be seen, both the RCT and NRCT results display an overall increasing trend with the increasing of the collision energy, while the RNCT probabilities drop slightly as the collision energy is increased. At $J = 0$, the threshold energy value of about 1.88 eV was observed for RCT which is smaller than the corresponding TSH value[17](note that although a different PES was used in TSH mothod, the relative large difference between 1.88 and 2.01 eV can be compared qualitatively) due to the quantum tunneling effect, and compared with the $(DH_2)^+$ system,[20] an isotopic effect has been shown from the larger threshold energy of the $(HD_2)^+$ system. The "energy shift" at large J's caused by the centrifugal barrier was also observed in the two processes. The probabilities of both RCT and RNCT decrease with an increasing total angular momentum nearly at each collision energy, whereas an abnormal J-dependent behavior of the probabilities is observed for the NRCT in which the probabilities do increase with increasing J for low J's of 0−10 and then decrease for higher J's, this abnormal behavior probably arises from that the centrifugal barriers caused by the low J values of 0−10 become higher to hinder the reaction, providing much more chance with increasing J for the reactant to be repelled backward, thus the nonreactive scattering probabilities increase, and the continued increase for J make the centrifugal barriers too high to access the crossing seam for charge transfer, in other word, not only the occurrence of reaction but also the charge-transfer processes are handicapped, so the probabilities decease of higher J's for NRCT channel.

Figure 3 demonstrates the effect of the initial vibrational excitation on the reaction probabilities for $J = 0$. A remarkable increase in the RCT/NRCT probabilities is observed at the vibrational excitation of $v = 3$ and 4 as compared with $v = 0$

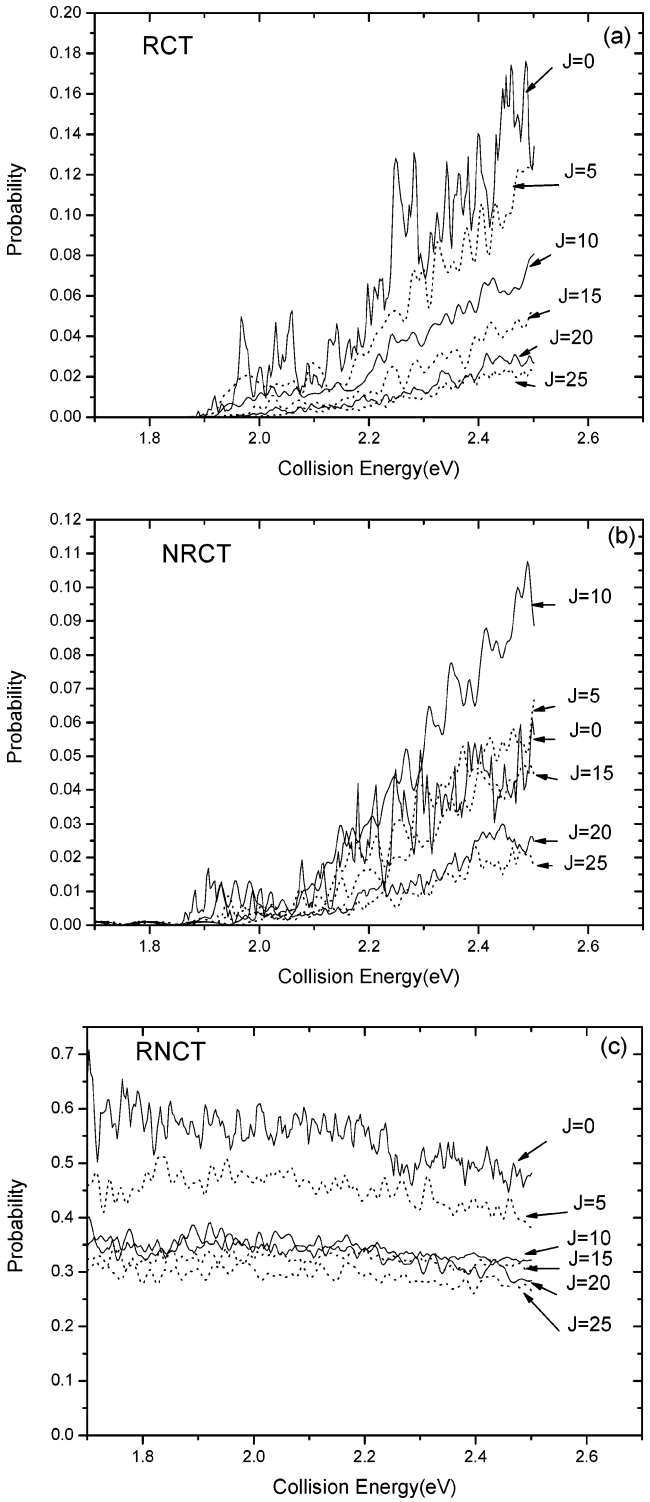

Figure 2. Dependence of the reaction probabilities on collision energy in the energy range of 1.7−2.5 eV with $J = 0$, 5, 10, 15, 20, and 25. (a) Probabilities of the RCT process $H^+ + D_2$ ($v = 0$, $j = 0$) → $D + HD^+$. (b) Probabilities of the NRCT process $H^+ + D_2$ ($v = 0$, $j = 0$) → $H + D_2^+$. (c) Probabilities of the RNCT process $H^+ + D_2$ ($v = 0$, $j = 0$) → $D^+ + HD$.

probabilities. The $v = 4$ probabilities are larger than $v = 3$ probabilities due to that the nonadiabatic transition occurs effectively in the reagent arrangement at the initial vibrational level closest to the crossing seam and $v = 4$ is the right vibrational level as can be seen explicitly in Figure 1. Meanwhile, the RNCT probability at $v = 3$ and 4 decreases to an average of 25% and 30%, respectively. In Figure 4, the sum

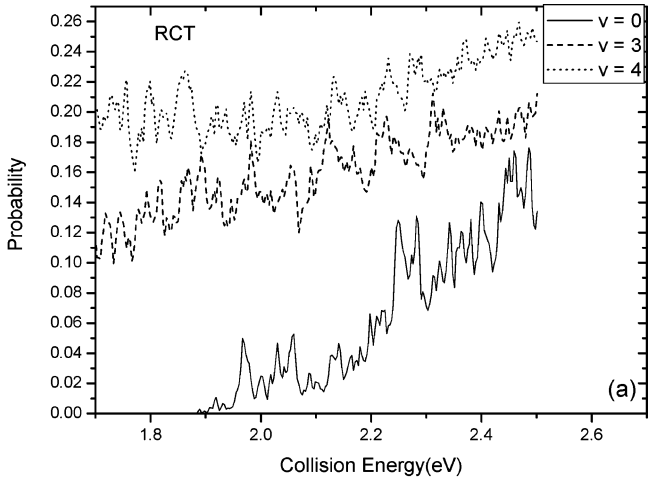

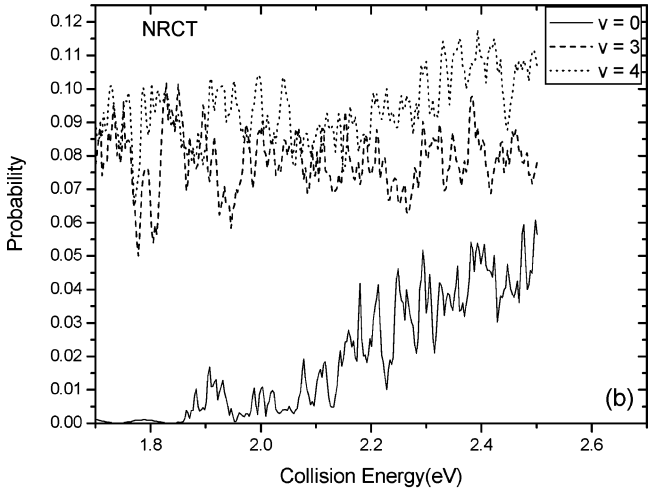

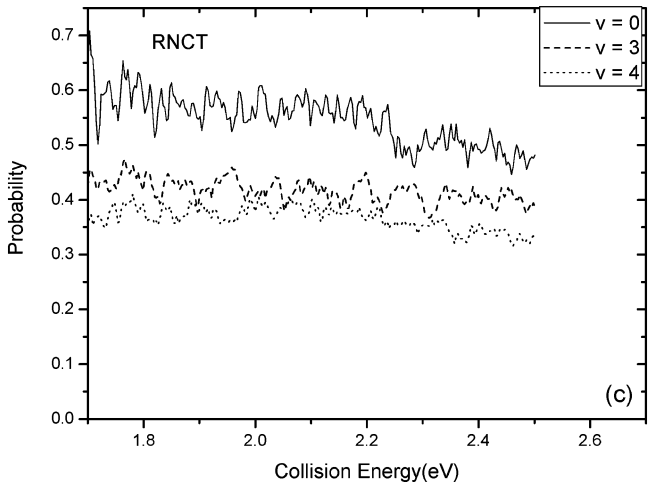

Figure 3. Reaction probabilities for $J = 0$ at vibrational levels $v = 0$, 3, and 4 with $j = 0$ of the reactant D_2, respectively: (a) the RCT process; (b) the NRCT process; (c) the RNCT process. Solid, dashed, and dotted lines correspond to $v = 0$, 3, and 4, respectively.

of the $v = 4$ RCT and NRCT probabilities is always smaller than the $v = 4$ RNCT probability until it becomes comparable to the RNCT probability at a collision energy of 2.35 eV, and this sum exceeds the RNCT probability only with the collision energy above 2.45 eV. Besides, the nonadiabatic probability of $v = 4$ was little enhanced by the translational excitation at collision energies below 2.2 eV, yet the enhancement occurred at higher collision energies. Such results show that the larger

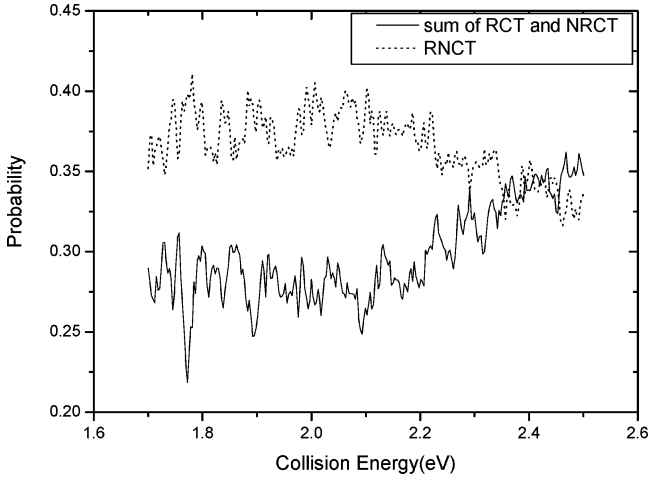

Figure 4. Comparison between the sum of the RCT and NRCT probabilities and the probability of RNCT at vibrational level $v = 4$ with $j = 0$ of the reactant D_2. The solid line shows the sum of RCT and NRCT probabilities, and the short-dotted line shows the probability of RNCT.

nonadiabatic probability at high collision energy in comparison with RNCT value for $v = 4$ probably arises from a joint effect of the vibrational excitation and the translational excitation, whereas the individual vibrational excitation of $v = 4$ only leads to a moderate increase in the nonadiabatic probabilities without exceeding the RNCT probability at most collision energies. It should be noted here that the vibrational excitation effects on the present $(HD_2)^+$ system are somewhat different from the previous $(DH_2)^+$ system in which the vibrational excitation of $v = 4$ caused the always larger nonadiabatic probability than the RNCT probabilities in the whole investigated collision energy range. For this, we again attribute to the isotopic mass effect of the reactant.

Figure 5 depicts the probabilities of the three channels for reaction $H^+ + D_2(v = 3, j = 0,2)$ and the total angular momentum J equals to zero. The rotational excitation on the three channels are quite different in that it has little effect on the RCT channel while it enhanced the NRCT to some extent and mildly decreases the RNCT probabilities. The results showed that the rotational excitation of the reactant could also enhance the nonadiabatic transition probabilities, particularly for the NRCT process.

The present results thus provided a quantum picture for the underlying reaction mechanism: analysis of the three reaction probabilities shows that this reaction is dominated by an insertion mechanism that occurred mainly on the ground $1^1A'$ surface. However, the two excited states $2^1A'$ and $3^1A'$ may also contribute to the underlying mechanism, especially for high initial vibrational and rotational levels of the reactant or at high collision energies. The general increasing trend of both RCT and NRCT probabilities with increasing collision energies, together with the decreasing trend of RNCT probability, suggests that the underlying mechanism is progressively mediated by a direct abstract mechanism for high collision energy. Furthermore, the v dependence and j dependence of the three calculated probabilities also revealed that the reaction occurred on the excited surfaces could be facilitated by the vibrational excitation or by the rotational excitation of the reactant D_2. Particularly, when the reactant is excited to its closest vibrational level of $v = 4$ to the surface crossing, the nonadiabatic transitions contribute most to the underlying mechanism of the reaction system.

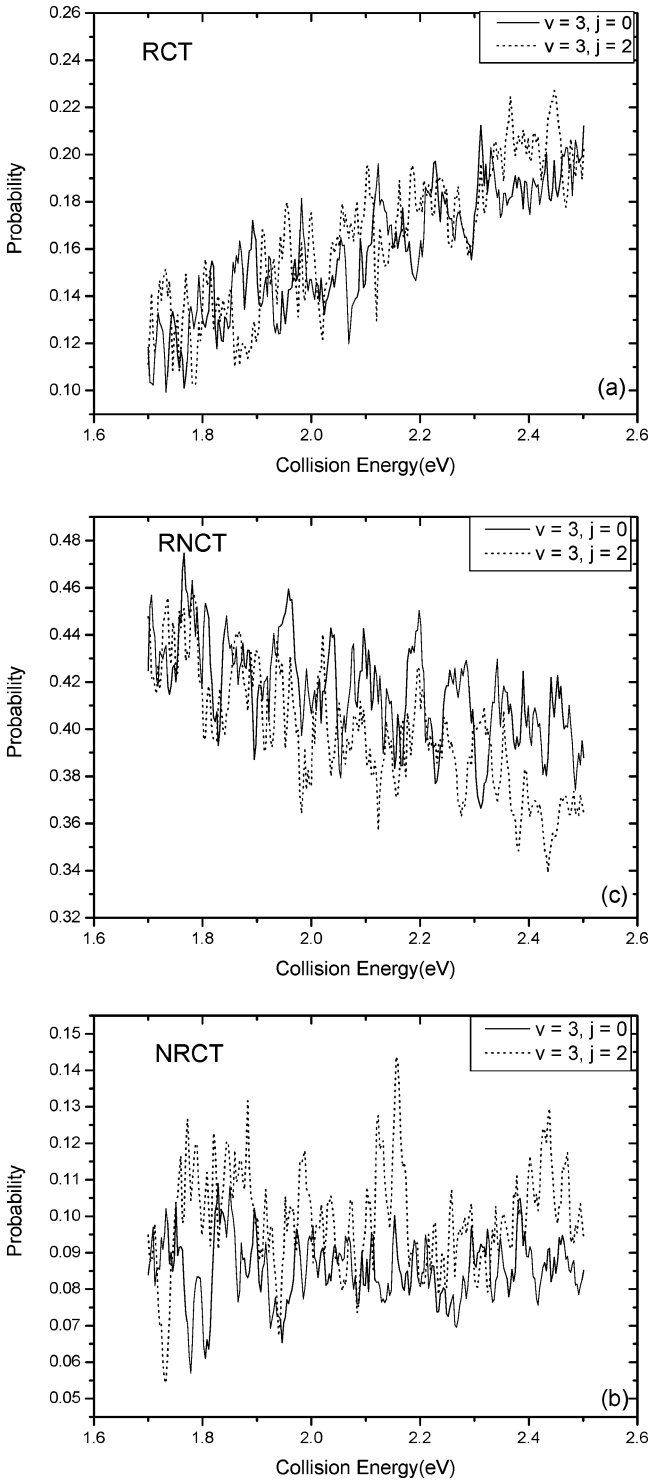

Figure 5. Calculated reaction probabilities as a function of collision energy for $H^+ + D_2$ ($v = 3$, $j = 0$, 2) and $J = 0$: (a) for RCT; (b) for NRCT; (c) for RNCT. Solid line denotes $j = 0$, and short-dotted line denotes $j = 2$.

The cross sections for the ground rovibrational initial state of D_2 are shown in Figure 6. In the calculated cross sections, the resonances still survive to some extent and leads to the observable wiggling structures. Overall, there is an increasing trend in the cross sections of the RCT and NRCT and a decreasing trend in the RNCT over the whole investigated energy range. The cross section of RCT shows noticeable threshold energy of about 1.90 eV, a little different from the threshold of 1.88 eV in the calculated probabilities. Again, the calculated cross sections as a function of the collision energy

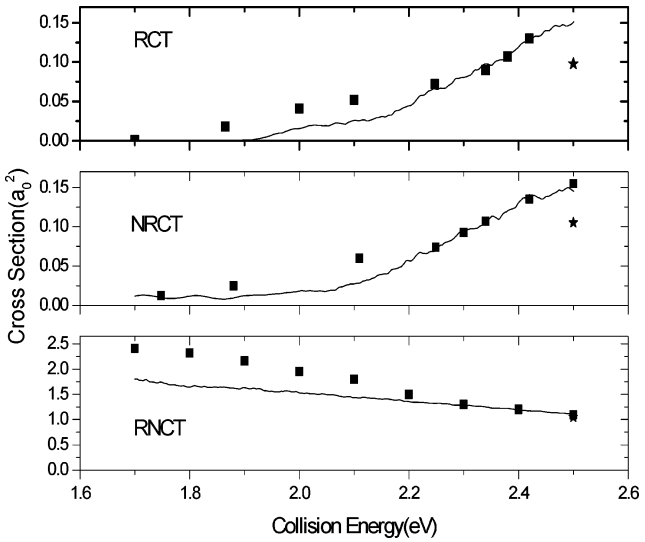

Figure 6. Present quantum cross sections in the collision energy range of 1.7−2.5 eV, compared with the experiment measurements of E. Teloy et al.[9] and the TSH calculations of Ichihara et al.[17] Solid line, solid squares, and solid star correspond to the present results, experimental data, and TSH results, respectively.

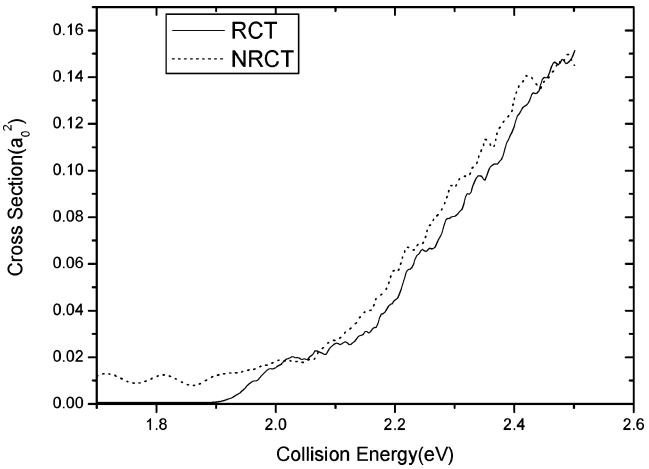

Figure 7. Comparison of cross sections between the two nonadiabatic processes of RCT and NRCT.

for the three channels provide an evidence for the dominant role of the ground $1^1A'$ surface and the roles of the excited surfaces in the reaction mechanism as we discussed above. We also present in Figure 6 the experimental cross sections[36] and the TSH calculated values[17] for all three processes. There is an overall agreement of the general trend in cross sections over all collision energies considered between the present quantum results and the experimental measurements, and the theoretical and the experimental results at higher collision energies are in better agreement than at lower collision energies. The present quantum cross sections of the nonadiabatic transitions are slightly larger than the corresponding TSH results. In addition, the present quantum calculation yields a threshold of about 1.90 eV for RCT, which is in better agreement with the experimental value of 1.86 eV than the TSH value of 2.01 eV.

The RCT/NRCT cross sections of $H^+ + D_2$ reaction (see Figure 7) do not display an alternative ascending fashion as in the case of the $(DH_2)^+$ reaction system in which the two nonadiabatic channels are very competitive.[20] It is observed that the NRCT cross section is slightly larger than the RCT cross section almost at each collision energy, indicating that in the present reaction system the chance for the reactant to repel

backward is a little larger than proceed forward to the product side and thus results in the slightly preference of the NRCT over the RCT in the two nonadiabatic processes of the same order in magnitudes. The reasons probably lies in that the heavy isotopic mass of the $(HD_2)^+$ system makes it rather difficult for the reactant to surmount the barriers on the excited surfaces to reach the product channels on the other side, which is necessary in the occurrence of the RCT process. It is also possible that the preference of the NRCT may arise from the contribution of the crossing seams located in the reactant channel since the crossing seams of the system are located both in the entrance and in the exit asymptotic regions.

IV. Conclusions

A three-dimensional nonadiabatic quantum calculation using the XSOS method to treat the multisurface scattering problems has been carried out for the three competing processes of the RCT, NRCT and RNCT in the $H^+ + D_2$ reaction system. This reaction system has a deep well on the ground surface, leading to numerous resonances in the calculated probabilities and these mapped out resonance structures are not washed out completely in the calculated cross sections. The RNCT is found to be the main channel for the ground rovibrational initial state of the reactant D_2, nevertheless, when D_2 is vibrationally or rotationally excited, in particular to its closest level to the surface crossing, the nonadiabatic processes could be enhanced to a large extent. Furthermore, a slight preference is found for NRCT in the two nonadiabatic processes which are of the same order of magnitude in cross sections. The exact quantum cross sections are found to be in good agreement with experimental results, and thus confirm the validity of the time-dependent wave packet method we used for treating the nonadiabatic processes in ion/atom−diatom collision dynamics.

Acknowledgment. This work was supported by NKBRSF (1999075302), the Knowledge Innovation Program of Chinese Academy of Sciences (INF105-SCE-02-08), and the NSFC (20373071, 20333050). The authors thank Professor Hiroki Nakamura for providing us the KBNN PES used in this study.

References and Notes

(1) Jasper, A. W.; Zhu, C. Y.; Nangia, S.; Truhlar, D. G. *Faraday Discuss.* **2004**, *127*, 1.
(2) Köppel, H. *Faraday Discuss.* **2004**, *127*, 35.
(3) Lee, S. H.; Dong, F.; Liu K. *Faraday Discuss.* **2004**, *127*, 49.
(4) Worth, G. A.; Robb, M. A.; Burghardt, I. *Faraday Discuss.* **2004**, *127*, 307.
(5) Yarkony, D. R. *Faraday Discuss.* **2004**, *127*, 325.
(6) Baer, M.; Ve'rtesi, T.; Halász, G. J.; Vibók, Á.; Suhai, S. *Faraday Discuss.* **2004**, *127*, 337.
(7) Tully, J. C. *Faraday Discuss.* **2004**, *127*, 463.
(8) Tully, J. C.; Preston, R. K. *J. Chem. Phys.* **1971**, *55*, 562.
(9) Ochs, G.; Teloy, E. *J. Chem. Phys.* **1974**, *61*, 4930.
(10) Schlier, C.; Nowotny, U.; Teloy, E. *Chem. Phys.* **1987**, *111*, 351.
(11) Last, I.; Gilibert, M.; Baer, M. *J. Chem. Phys.* **1997**, *107*, 1451.
(12) Ushakov, V. G.; Nobusada, K.; Osherov, V. I. *Phys. Chem. Chem. Phys.* **1996**, *3*, 63.
(13) Markovic, N.; Billing, G. D. *Chem. Phys. Lett.* **1996**, *248*, 420.
(14) Markovic, N.; Billing, G. D. *Chem. Phys.* **1995**, *191*, 247.
(15) Billing, G. D.; Markovic, N. *Chem. Phys.* **1996**, *209*, 377.
(16) Takayanagi, T.; Kurosaki, Y.; Ichihara, A. *J. Chem. Phys.* **2000**, *112*, 2615.
(17) Ichihara, A.; Shirai, T.; Yokoyama, K. *J. Chem. Phys.* **1996**, *105*, 1857.
(18) Ichihara, A.; Yokoyama, K. *J. Chem. Phys.* **1995**, *103*, 2109.
(19) Kamisaka, H.; Bian, W.; Nobusada, K.; Nakamura, H. *J. Chem. Phys.* **2002**, *116*, 654.
(20) Chu, T. S.; Han, K. L. *J. Phys. Chem. A* **2005**, *109*, 2050.
(21) Viegas, L. P.; Cernei, M.; Alijah, A.; Varandas, A. J. C. *J. Chem. Phys.* **2004**, *120*, 253.
(22) Friedrich, O.; Alijah, A.; Xu, Z. R.; Varandas, A. J. C. *Phys. Rev. Lett.* **2001**, *86*, 1183.
(23) Tully, J. C. *J. Chem. Phys.* **1974**, *60*, 3042.
(24) Honvault, P.; Launay, J. M. *Chem. Phys. Lett.* **1999**, *303*, 657.
(25) Alexander, M. H.; Manolopoulos, D. E.; Werner, H. J. *J. Chem. Phys.* **2000**, *113*, 11084.
(26) Zhang, Y.; Xie, T. X.; Han, K. L. *J. Phys. Chem. A* **2003**, *107*, 10893.
(27) Schatz, G. C. *J. Phys. Chem.* **1995**, *99*, 7522.
(28) Schatz, G. C.; McCabe, P.; Connor, J. N. L. *Faraday Discuss.* **1998**, *110*, 139.
(29) Hoffmann, M. R.; Schatz, G. C. *J. Chem. Phys.* **2000**, *113*, 9456.
(30) Maiti, B.; Schatz, G. C. *J. Chem. Phys.* **2003**, *119*, 12360.
(31) Gray, S. K.; Goldfield, E. M.; Schatz, G. C.; Balint-Kurti, G. G. *Phys. Chem. Chem. Phys.* **1999**, *1*, 1141.
(32) Balint-Kurti, G. G.; Gonzalez, A. I.; Goldfield, E. M.; Gray, S. K. *Faraday Discuss.* **1998**, *110*, 169.
(33) Zhang, H.; Smith, S. C. *Phys. Chem. Chem. Phys.* **2004**, *6*, 4240.
(34) Zhang, H.; Smith, S. C. *J. Chem. Phys.* **2004**, *120*, 9583.
(35) Lin, S. Y.; Guo, H. *J. Chem. Phys.* **2004**, *121*, 1285.
(36) Lin, S. Y.; Guo, H. *J. Phys. Chem. A* **2004**, *108*, 2141.
(37) Kosloff, R. J. *J. Phys. Chem.* **1988**, *92*, 2087.
(38) Zhang, D. H.; Zhang, J. Z. H. In *Dynamics of Molecules and Chemical Reactions*; Wyatt, R. E., Zhang, J. Z. H., Eds.; Marcel Dekker: New York, 1996; Chapter 6.
(39) Yang, B. H.; Tang, B. Y.; Yin, H. M.; Han, K. L.; Zhang, J. Z. H. *J. Chem. Phys.* **2000**, *113*, 7182.
(40) Zhang, X.; Yang, G. H.; Han, K. L.; Wang, M. L.; Zhang, J. Z. H. *J. Chem. Phys.* **2003**, *118*, 9266.
(41) Zhang, J. Z. H.; Dai, J.; Zhu, W. *J. Phys. Chem. A* **1997**, *101*, 2746.
(42) Xie, T. X.; Zhang, Y.; Zhao, M. Y.; Han, K. L. *Phys. Chem. Chem. Phys.* **2003**, *5*, 2034.
(43) Zhang, Y.; Xie, T. X.; Han, K. L.; Zhang, J. Z. H. *J. Chem. Phys.* **2003**, *119*, 12921.
(44) Zhang, Y.; Xie, T. X.; Han, K. L. *J. Phys. Chem. A* **2003**, *107*, 10893.
(45) Zhang, Y.; Xie, T. X.; Han, K. L.; Zhang, J. Z. H. *J. Chem. Phys.* **2004**, *120*, 6000.
(46) Alexander, M. H.; DePristo, A. P. *J. Chem. Phys.* **1977**, *66*, 2166.
(47) Zhang, D. H.; Zhang, J. Z. H. *J. Chem. Phys.* **1993**, *99*, 6624.